Journal of Catalysis **211,** 482–495 (2002)
doi:10.1006/jcat.2002.3759

Oxidative Dehydrogenation of Propane over Supported Chromia Catalysts: Influence of Oxide Supports and Chromia Loading

Maymol Cherian,* Musti Someswara Rao,* Andrew M. Hirt,† Israel E. Wachs,‡ and Goutam Deo*,[1]

*Department of Chemical Engineering, Indian Institute of Technology, Kanpur, 208 016 India; †Material Research Laboratory, Inc., 290 North Bridge Street, Struthers, Ohio 44471; and ‡Zettlemoyer Center for Surface Studies, Department of Chemical Engineering, Lehigh University, Bethlehem, Pennsylvania 18015

Received April 19, 2002; revised July 18, 2002; accepted July 22, 2002

Several loadings of chromium oxide ranging from sub- to above monolayer coverages were prepared on various oxide supports and characterized by various techniques. From a combination of Raman, XPS, and DRS characterization studies the monolayer surface coverages were determined to be ∼12, ∼4, ∼1, and ∼3% Cr_2O_3 on the Al_2O_3, TiO_2, SiO_2, and SiO_2–Al_2O_3 supports, respectively. *In situ* Raman and DRS characterization studies under dehydrated conditions revealed the presence of dispersed surface Cr^{6+} oxide species for samples below monolayer loadings. Additional Cr^{5+} and δ-Cr^{3+} species were detected by EPR. From the TPR studies, the reducibility of the surface chromium oxides (T_{max}) was decreasing in the order $TiO_2 < SiO_2$–$Al_2O_3 \sim Al_2O_3 < SiO_2$. The reactivity studies using the oxidative dehydrogenation of propane revealed that the activity and propene selectivity of the supported chromia catalysts depend on the loading and the oxide support used. The highest activity was obtained on the Cr_2O_3/Al_2O_3 sample, since the largest amount of chromium oxide could be dispersed on the supports. The selectivity to propene at monolayer coverages was similar for the CrAl and CrTi samples, since at these coverages exposed support sites are unavailable for degrading propene. For the CrSi and CrSiAl samples, however, a significant amount of support is exposed for degrading propene. The intrinsic activity of the surface chromium oxide species, the TOF values, follows the trend CrTi ≅ CrSi > CrSiAl ≥ CrAl. There is a difference between the variation in TOF values and the reducibility of the supported chromium oxide catalysts. Thus, it appears that the reducibility of the catalyst is not the only factor that is important in determining the activity of the surface chromium oxide species. Furthermore, based on the dispersion amount of chromium oxide on the different oxide supports, the CrTi catalysts appear to be the most suitable among the catalysts studied for the ODH of propane.

Key Words: **chromia; ODH; propane; TPR; EPR; Raman; DR UV–vis; TOF; activity; propene selectivity.**

INTRODUCTION

Conversion of alkanes into their corresponding alkenes is an industrially important process due to the increased demand for alkenes. It is currently achieved by catalytic dehydrogenation over alumina-supported chromia catalysts. Despite its simplicity the application of catalytic dehydrogenation is limited due to thermodynamic constraints. Most of the limitations of the dehydrogenation reactions can be overcome by employing oxidative dehydrogenation (1). The activation of alkanes is, however, more difficult than that of the corresponding alkenes. Consequently, the alkene formed is more susceptible to over-oxidation to carbon oxides. Maximizing the formation of alkenes is, therefore, a critical issue for oxidative dehydrogenation reactions. It requires a catalyst that would significantly accelerate the abstraction of hydrogen from the alkane molecule and hinder both the nucleophilic insertion of oxygen into the molecule and the electrophillic attack of oxygen molecules on the C–C bonds (2).

Supported and unsupported transition metal oxides have been widely used for the selective oxidation of hydrocarbons. For example, vanadium- and molybdenum oxide-based catalysts have been successfully used for numerous selective oxidation reactions. Oxides such as MnO_2, V_2O_5, Co_3O_4, CuO, Cr_2O_3, TiO_2, ZrO_2, WO_3, and CeO_2 as bulk or in binary or multiple compositions have also been employed for oxidation of hydrocarbons (3, 4). The catalytic activity of these oxides depends on their surface structure, character of chemical bonds, and coordinative unsaturation of the active surface site. In recent years supported metal oxides have gained much attention due to their high degree of mechanical strength, better thermal stability, and larger surface area (5). Vanadia- and molybdena-based catalysts supported on Al_2O_3, TiO_2, ZrO_2, and SiO_2 have been widely studied for alkane oxidative dehydrogenation reactions (6–10). It was observed that the two-dimensional monolayer surface metal oxide species present on the support is more active than the respective bulk metal oxides

[1] To whom correspondence should be addressed. Fax: +91-512-590104. E-mail: goutam@iitk.ac.in.

0021-9517/02 $35.00

for oxidative dehydrogenation reactions. Furthermore, supported vanadia catalysts have been reported to be very active catalysts for alkane ODH, but their selectivity was found to be somewhat lower.

Supported chromia catalysts have also been successfully studied for dehydrogenation and oxidative dehydrogenation reactions (11–15). For example, Grzybowska *et al.* (16) and Al-Zahrani *et al.* (17) studied the influence of chromia loading and preparation methods on the structure–reactivity properties of Cr_2O_3/Al_2O_3 catalysts for the ODH of isobutane. They observed an optimum chromium loading on Al_2O_3 (surface area = 245 m^2/g) between 5 and 15 wt% of Cr_2O_3, where the ODH activity was the highest. Hoang *et al.* (18) carried out the ODH of isobutane over chromia supported on different oxide supports and observed a higher conversion and selectivity for the $La(CO_3)_3$-supported chromia catalyst. Grabowski *et al.* (19) reported that the intrinsic activity for the ODH of isobutane is high for chromia supported on TiO_2 catalysts. Furthermore, the selectivity for CrO_x/TiO_2 and potassium-promoted CrO_x/Al_2O_3 catalysts were higher than that for CrO_x/Al_2O_3 catalysts. Stoczynski *et al.* (20), however, reported a higher selectivity and conversion for the CrO_x/Al_2O_3 than the CrO_x/TiO_2 catalysts during the ODH of isobutane. Most of these studies were primarily aimed at understanding the effect of the oxide support and limited to analysis of a single loading of chromium oxide. Information regarding the effect of chromium oxide loading, however, was sparse.

The nature of the chromium oxide species in supported chromium oxide catalysts is known to depend on the loading and specific oxide support. Various characterization techniques have been applied to study the supported chromium oxide phase on different oxide supports: XRD, Raman, TPR, XPS, ESR, and UV–vis studies (21–27). From these characterization techniques it has been determined that the supported chromia catalysts possess a two-dimensional surface chromia species below monolayer loadings. The oxide support–surface chromia interaction stabilizes the Cr species in different oxidation states (Cr^{2+}, Cr^{3+}, Cr^{5+}, and Cr^{6+}). The relative stability of the different chromia oxidation states depends on the extent of support–surface chromia interaction, on the acid–base properties of the support, and on the interaction energy between the surface chromia–support phases (28). It has been proposed that the surface chromium oxide species are predominantly present in the +6 oxidation state under oxidizing conditions (29).

For a better understanding of the behavior of supported chromium oxide catalysts it is necessary to simultaneously study the effect of chromia loading and of the specific oxide support on the reactivity of propane ODH. The primary focus of the present study is to understand the effect of loading and support on the reactivity of the surface chromia species toward the ODH of propane. To achieve this goal several loadings of chromium oxide ranging from sub- to above monolayer coverages were prepared on several oxide supports (Al_2O_3, TiO_2, SiO_2, and SiO_2–Al_2O_3). The synthesized samples were molecularly characterized and investigated for the ODH of propane to fundamentally understand the structure–reactivity relationship of the supported chromium oxide catalysts.

EXPERIMENTAL

Catalyst Preparation

The supported chromia catalysts were prepared by the incipient wetness impregnation technique. The precursor used was chromium nitrate nonahydrate ($Cr(NO_3)_3 \cdot 9H_2O$, Aldrich, 99.98% purity). Commercial alumina (Condea), titania (Degussa, P-25), silica (Condea), and silica–alumina (Condea, 30 wt% silica) were used as the oxide supports. The supports were pretreated with incipient volumes of distilled water and then calcined for 6 h at 600°C for the alumina, silica, and silica–alumina and at 450°C for titania supports. The pretreated supports and incipient volumes of aqueous solutions containing predetermined amounts of the chromium nitrate precursor were intimately mixed in order to prepare the catalysts with different loadings of chromium oxide. The mixture was kept in a dessicator overnight, followed by drying at 110°C for 8 h and at 250°C for another 8 h. Finally the samples were calcined at 600 or 450°C for 6 h, depending on the support. The prepared catalysts were denoted as x% CrAl, x% CrTi, x% CrSi, and x% CrSi–Al, where x% is the wt% loading in terms of Cr_2O_3.

Surface Area

The surface areas of the samples were obtained using the single-point BET method. A bench-top COULTER SA 3100 apparatus using N_2 adsorption at 77 K was used for this purpose.

Raman Spectroscopy

The laser Raman spectroscopy studies of the supported chromia catalysts under ambient and dehydrated conditions were obtained by means of a 514-nm line of an argon ion laser excitation source. The Raman apparatus consisted of a Triplemate spectrometer (Spex Model 1877) coupled to an optical multichannel analyzer (OMA III, Princeton Applied Research, Model 1463). The laser power at the sample was ~50 mW. About 200 mg of the supported chromia catalysts was pressed into self-supporting wafers and placed in a rotating sample cell to avoid local heating effects. The dehydrated Raman spectra were obtained using a stationary *in situ* Raman cell using the same protocol as Vuurman *et al.* (30).

X-Ray Photoelectron Spectroscopy (XPS)

X-ray photoelectron spectroscopy (XPS) studies were done using Mg K_α or Al K_α in fixed analyser transmission (FAT) mode. The catalyst powder was pressed between a stainless-steel holder and a polished single-crystal silicon wafer, which was installed in a vacuum chamber of a Model DS 800 XPS surface analysis system manufactured by Kratos Analytical, Manchester, UK.

Electron Paramagnetic Resonance (EPR)

Electron paramagnetic resonance studies were performed on a Varian E-109 X band spectrometer. The spectra were obtained under ambient conditions using a microwave frequency of ~9.15 GHz and a microwave power of 10 mW. The scan time was 8 min and the magnetic field modulation frequency was 100 kHz. The EPR spectra were calibrated with DPPH using a duel cell. Samples before and after the propane ODH reaction were studied by EPR spectroscopy. The samples after propane ODH reaction were exposed to ambient conditions before the EPR spectra were obtained.

Diffusive Reflectance Spectroscopy (DRS)

Diffuse reflectance ultraviolet–visible spectroscopy (DR UV–vis) studies of the chromia supported on alumina catalysts were performed on a Varian Cary 5E UV–vis NIR spectrophotometer. The spectra were obtained under ambient and dehydrated conditions using a Harrick DRS cell with the praying mantis diffuse reflectance attachment (DRA). Spectra from 200 to 800 nm were collected and referenced with alumina. Prior to obtaining the DRS, the samples were calcined at 500°C and then diluted at room temperature with alumina to a weight ratio 1 : 10. The diluted sample was loaded into the DRS cell, and the temperature was increased from room temperature to 100, 200, 300, 400, and 500°C and finally decreased to room temperature in a stream of pure oxygen. The samples were kept at each temperature for 10 min and then the spectrum was taken.

The diffuse reflectance spectra of the surface chromium oxide species on alumina were also performed under *in situ* conditions during propane reduction. The reduction studies were carried out in ~30% propane in a helium stream. A procedure similar to that above was followed. After cooling the sample to room temperature in pure oxygen the gas stream was switched to the premixed 30% propane in helium stream and the temperature was changed again as above.

Temperature Programmed Reduction (TPR)

The TPR studies were carried out in a microreactor containing ca. 0.05 g of catalyst and attached to a Micromeritics Pulse Chemisorb 2705 analyzer. Helium was used as the carrier gas and also to degas the samples. Degassing of the sample was done for 0.5 h at 250°C prior to the reduction experiments. The helium flow was set at 30 ml/min. A 10% H_2/Ar mixture flowing at 40 ml/min was used for reduction and the temperature was ramped at a rate of 10°C/min from ~100 to 700°C. Hydrogen consumed was determined with a TCD. Known amounts of pure hydrogen were injected for quantification purposes.

Oxidative Dehydrogenation (ODH) of Propane

The samples were tested for the ODH of propane in a vertical downflow quartz reactor at atmospheric pressure. The reactor was a single quartz piece with an inlet 10 mm in internal diameter and 15 cm long and an outlet 5 mm in internal diameter and 15 cm long. The two sections were tapered and the catalyst bed was placed just above the tapered region on quartz wool. The reactor tube was mounted vertically in a tubular furnace. The temperature of the reactor and the catalyst bed was measured by a thermocouple located inside the reactor tube just above the catalyst bed and controlled by a PID temperature controller (FUJI Micro-controller X Model PXZ 4). The exiting gases were analyzed with a gas chromatograph (AIMIL-NUCON 5765) equipped with a methanizer. The carbon oxides and hydrocarbons were analyzed in FID mode using an activated alumina column. The propane flow was adjusted through a separate thermal mass flow controller (Bronkhost Hi-Tec, Model F-201D FAC-22-V) and the air flow rate was adjusted through a rotameter (Eureka, Model SRS/MG-5) to maintain a 3 : 1 propane-to-oxygen ratio. The feed composition in volume percent was maintained at ~35 propane, ~11.7 oxygen, and balance nitrogen. A physical mixture of 0.1 g of the catalyst and the amount of quartz glass powder required to form a bed height of 1 cm was loaded into the reactor. Runs were performed at different temperatures, starting from 300 to 450°C, with a constant total flow rate of 42.7 sccm. The conversions were maintained below 5% to ensure differential reaction conditions. Calculations based on published criteria (31) reveal that no heat and mass transfer limitations exist.

Based on the inlet and outlet concentrations and assuming differential reactor conditions the conversion, activity, selectivity, yield, and TOF values were calculated as

$$\text{Conversion } (\%) = (n_c/n_f) \times 100,$$
$$\text{Activity (moles of } C_3H_8 \text{ converted/g} \cdot \text{s)} = F_{A0} * X_A,$$
$$\text{Selectivity } (\%) = (n_{hc}/n_c) \times (N_{hc}/N_p) \times 100,$$
$$\text{Yield } (\%) = (n_{hc}/n_f) \times (N_{hc}/N_p) \times 100,$$
$$\text{TOF } (s^{-1}) = F_{A0} * X_A/n_{Cr},$$

where n_c, n_f are the number of moles of propane consumed and propane fed, respectively, n_{hc} is the number of moles of products (e.g., propene, ethene, carbon oxides, etc.) formed, N_{hc} and N_p are the number of carbon atoms present in the

products formed and in propane, respectively, F_{A0} is the moles of propane fed per second, X_A is the conversion of propane per gram of the catalyst, and n_{Cr} is the moles of Cr per gram of the catalyst.

Blank reactor runs were conducted and no significant conversions were observed under the present experimental conditions. Furthermore, the pure supports, such as Al_2O_3, TiO_2, SiO_2, and SiO_2–Al_2O_3 were observed to be inactive for ODH of propane under the present experimental conditions. For each catalyst several runs were taken and the average value is reported. The activation energies were calculated assuming differential reaction conditions in the temperature range of 380 to 450°C.

RESULTS

Several loadings of chromia were prepared on the oxide supports. The prepared samples were then analyzed for their surface area and further characterized using Raman, XPS, and EPR spectroscopic techniques. DRS studies of Cr_2O_3/Al_2O_3 catalysts were done in detail. The samples were then studied by TPR and ODH of propane. The results of these studies are presented below.

Surface Area

The surface areas of the pure oxide supports and chromium oxide supported on Al_2O_3, TiO_2, SiO_2, and SiO_2–Al_2O_3 were determined and are tabulated in Table 1. The surface area for the four sets of supported chromium oxide samples decreased with chromia loading and remained relatively constant for higher loadings. For example, the surface area of the CrAl samples decreased from 200 to ~155 m^2/g, the CrTi samples decreased from 60 to 40 m^2/g, the CrSi samples decreased from 223 to ~170 m^2/g, and the CrSiAl samples decreased from 360 to ~180 m^2/g. Similar variations in surface area with loading have been reported by others (13, 18).

Raman Studies

The ambient Raman spectra for different loadings of chromia supported on alumina, CrAl, are shown in Fig. 1.

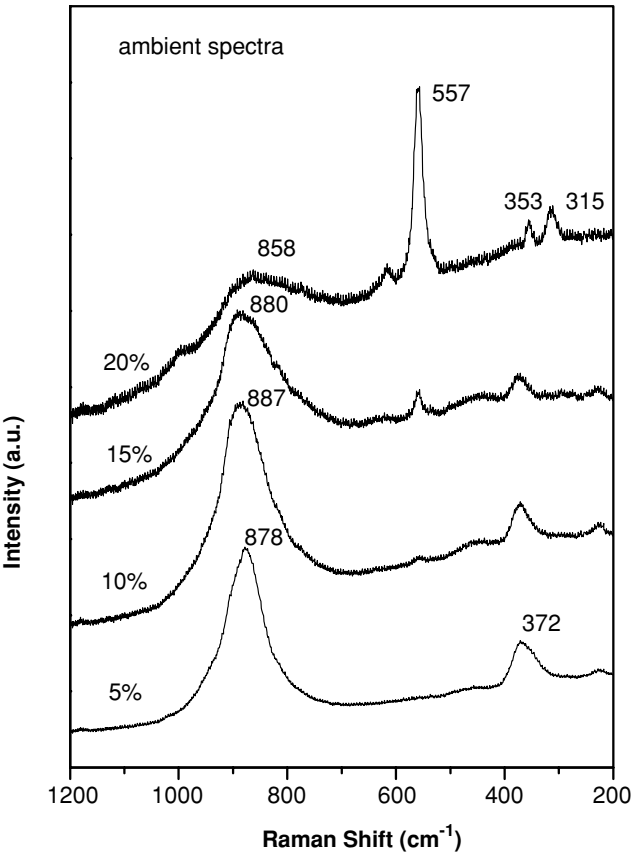

FIG. 1. Raman Spectra of x% CrAl samples obtained under ambient conditions.

The major Raman band is observed between 800 and 900 cm^{-1}. Raman bands at 350 and 220 cm^{-1} were also observed. From the published literature, these bands correspond to hydrated 4-coordinated chromium oxide species in the Cr^{6+} oxidation state (32). As the chromia loading increases up to 15%, a shift toward higher frequency is observed for the 800- to 900-cm^{-1} band corresponding to an increase in polymerization of the hydrated surface chromium oxide species. For 15 and 20% chromia loadings a new band is also present, at 557 cm^{-1}, which corresponds to crystals of Cr_2O_3.

TABLE 1

Surface Area of Supported Chromia Catalysts

Samples	Surface area (m^2/g)	Samples	Surface area (m^2/g)	Samples	Surface area (m^2/g)	Samples	Surface area (m^2/g)
Al_2O_3	201	TiO_2	60	SiO_2	223	SiO_2–Al_2O_5	360
5 CrAl	189	1 CrTi	41	0.5 CrSi	206	0.5 CrSiAl	266
10 CrAl	156	3 CrTi	39	1 CrSi	202	1 CrSiAl	265
15 CrAl	140	5 CrTi	40	2 CrSi	168	2 CrSiAl	ND[a]
20 CrAl	155	7 CrTi	39	5 CrSi	170	5 CrSiAl	182
		10 CrTi	41				

[a] ND, Not determined.

TABLE 2

Raman Band Positions Under Ambient Conditions for Supported Chromium Oxide Species

Wt% CrAl	Raman band (cm^{-1})	Wt% CrTi	Raman band (cm^{-1})	Wt% CrSi	Raman band (cm^{-1})	Wt% CrSiAl	Raman band (cm^{-1})
5	878, 372	1	886, 800	0.5	865, 295	0.5	899, 363
10	887, 370	2	880	1	870, 300	1	894, 368
15	880, 558, 353	3	875, 800	2	978, 876, 619, 558, 355, 305	2	881, 372
20	858, 600, 557, 353, 315	5	859	5	870, 615, 558, 355, 305	5	876, 620, 558, 363

Similar to the CrAl samples, Raman bands due to chromium oxygen vibrations were observed for titania, silica, and silica–alumina-supported chromia catalysts. The major band position for CrTi, CrSi, and CrSi-Al catalysts are shown in Table 2. For the CrTi catalysts a broad band between 850 and 900 cm^{-1} and a shoulder at ~950 cm^{-1} is observed. These bands correspond to the Cr–O stretching vibrations of monochromates and polychromates. Due to the strong titania-supported Raman bands below ~800 cm^{-1}, the lower wave number bands of the surface chromia species cannot be observed for the CrTi catalysts. The major Raman band of the hydrated surface chromia species on the CrSi catalysts is centered at 875 cm^{-1} and a new Raman band is also present, at 558 cm^{-1}, for 2% and higher chromia loadings, which correspond to Cr_2O_3 microcystals. For the CrSiAl catalysts a sharp band is present at ~890 cm^{-1}, corresponding to the hydrated surface chromate species. The cystalline Cr_2O_3 band is detected for the 5% CrSiAl sample.

The dehydrated Raman spectra for 10% CrAl, 3% CrTi, and 0.5% CrSi samples were also measured. The dehydrated surface chromia Raman spectra are dramatically different from those obtained under ambient conditions. New Raman bands at ~1002 cm^{-1} for 10% CrAl and 3% CrTi and at ~980 cm^{-1} for 0.5% CrSi were detected. Additional broad bands were observed at ~880 cm^{-1} for the 10% CrAl sample. The dehydrated spectra are not shown, for brevity, since similar spectra have been reported elsewhere (30).

XPS Studies

The XPS surface region analysis of the dehydrated chromia supported on alumina, titania, silica, and silica–alumina catalysts reveal the presence of only Cr, O, C, and *S* on the samples, where *S* is the support metal cation (Al, Ti, Si, or SiAl) present. Trace amounts of surface F, Cl, and Sn impurities were also detected. From the XPS data the surface atomic concentration of Cr and *S* were calculated and the $Cr/(Cr + S)_{surface}$ ratios were determined. For the CrSiAl samples the sum of Si and Al was taken as *S* since the Si : Al ratio from XPS is ~0.6 for all these samples. From knowledge of the amount of chromia contained in the sample the $Cr/(Cr + S)_{bulk}$ ratios were also calculated. The $Cr/(Cr + S)_{surface}$ ratio is plotted versus the $Cr/(Cr + S)_{bulk}$ ratio in Fig. 2. It is observed from Fig. 2 that the $Cr/(Cr + S)_{surface}$ ratios increase with the $Cr/(Cr + S)_{bulk}$ ratio and then attain a relatively constant value, except for the CrSi samples. For the CrSi catalysts the $Cr/(Cr + S)_{surface}$ ratio is almost constant for the different $Cr/(Cr + S)_{bulk}$ values.

EPR Studies

The EPR spectra of the *x*% CrAl, CrTi, CrSi, and CrSiAl calcined catalysts were obtained before and after the propane ODH reaction. The effect of loading on the EPR signal for the 0.5, 1, 5, 7.5, and 10% CrAl catalysts before reaction is shown in Fig. 3. For samples up to 7.5% Cr_2O_3 loading a strong axially symmetric peak with a *g*-value = 1.97 and $\Delta H = 50$ was observed. This peak has been assigned to the γ-signal of isolated axially symmetric Cr^{5+} species (21). For the 10% CrAl catalyst a broad spectra with

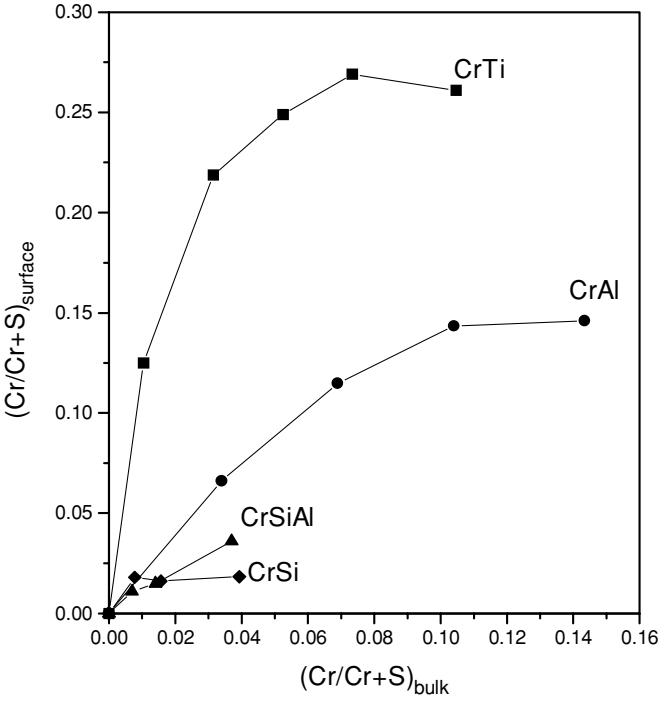

FIG. 2. $(Cr/Cr + S)_{surface}$ obtained from XPS versus $(Cr/Cr + S)_{bulk}$ for the different supported chromium oxide catalysts.

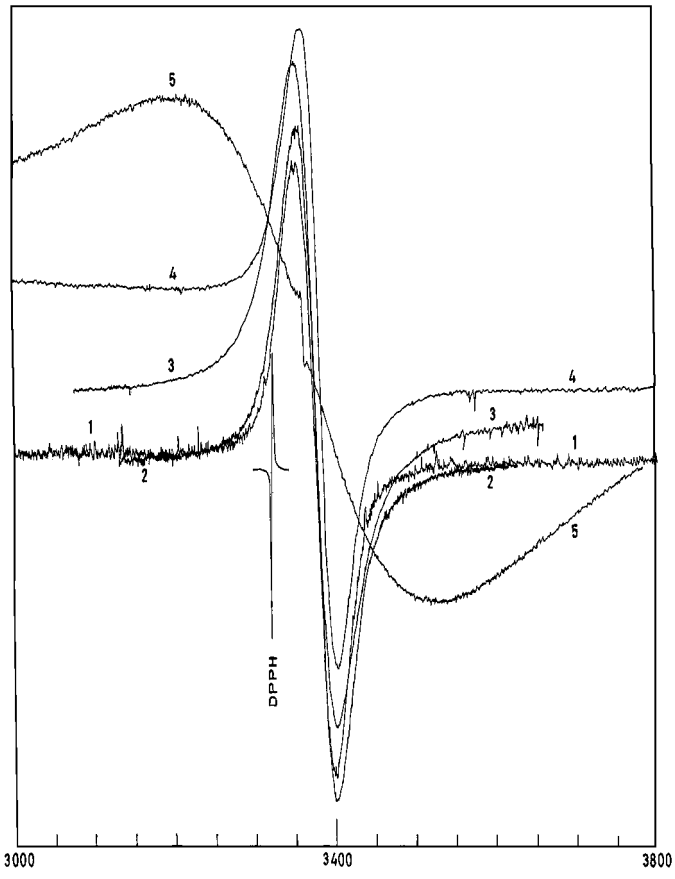

FIG. 3. EPR spectra under ambient conditions obtained for various CrAl samples before ODH of propane. Legend: 1, 0.5%; 2, 1%; 3, 5%; 4, 7.5%; 5, 10%.

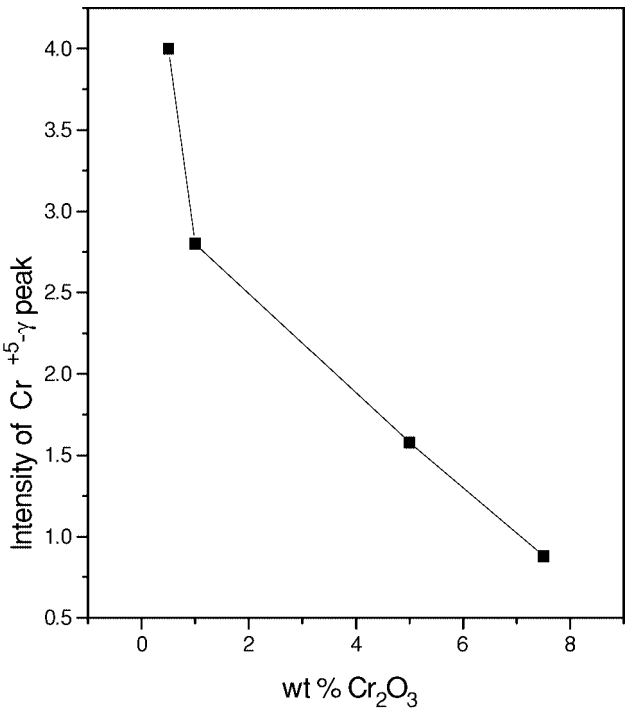

FIG. 4. Intensity of the Cr^{5+} γ-signal as a function of chromium oxide loading for different CrAl catalysts.

$g = 1.97$ and $\Delta H = 850$ G was observed in addition to the Cr^{5+} peak. This broad peak has been assigned to the β-Cr^{3+} signal due to Cr_2O_3 crystals (25). Due to the increase in intensity of the β-Cr^{3+} signal with loading, the γ-signal due to the Cr^{5+} species is not clearly identified for loadings higher than 10% Cr_2O_3 and is not shown.

The intensity of the peak corresponding to the Cr^{5+} γ-signal normalized for gain, microwave power, modulation amplitude, and weight of the chromium oxide taken for EPR analysis is plotted verus weight percent Cr_2O_3 loading in Fig. 4. From Fig. 4 it is observed that the γ-signal intensity decreases with an increase in chromia loading. Similarly, the EPR spectra of CrTi, CrSi, and CrSiAl catalysts before reaction also revealed the presence of Cr^{5+} species that monotonically decreases with an increase in loading. In addition to the Cr^{5+} and β-Cr^{3+} peaks, a third peak with a g-value $= 2.4$ was observed for 2% CrTi, 1% CrSiAl, 0.5% CrSi, and higher loadings on the TiO_2, SiO_2, and SiO_2–Al_2O_3 supports. However, this peak is absent for CrAl catalysts. This peak has been assigned to an isolated and dispersed δ-Cr^{3+} surface species (33). The g-value and linewidth, ΔH, corresponding to the different Cr species for the x% CrAl, CrTi, CrSi, and CrSiAl catalysts are presented in Table 3. The g-value corresponding to Cr^{5+} is the

TABLE 3

***g* and ΔH Values from the EPR Spectra of Supported Chromium Oxide Catalysts**

CrAl			CrTi			CrSiAl			CrSi		
Wt%	ΔH	g	Wt%	ΔH	g	Wt%	ΔH	g	Wt%	ΔH	g
0.5	50	1.97	0.5	30	1.97	0.5	40	1.97, 2.41	0.5	40	1.97
1	48	1.97	1	20	1.97	1	38	1.97, 2.41	1	40	1.97, 2.42
5	56	1.97	2	23	1.97, 2.37	2	32	1.97	2	38	1.97, 2.42
7.5	53	1.97	3	20	1.97, 2.37	5	50	1.97	5	40	1.97
	60, 850	1.97, 1.97	4	40	1.97, 2.37						
10											
			5	56	1.97, 2.37						

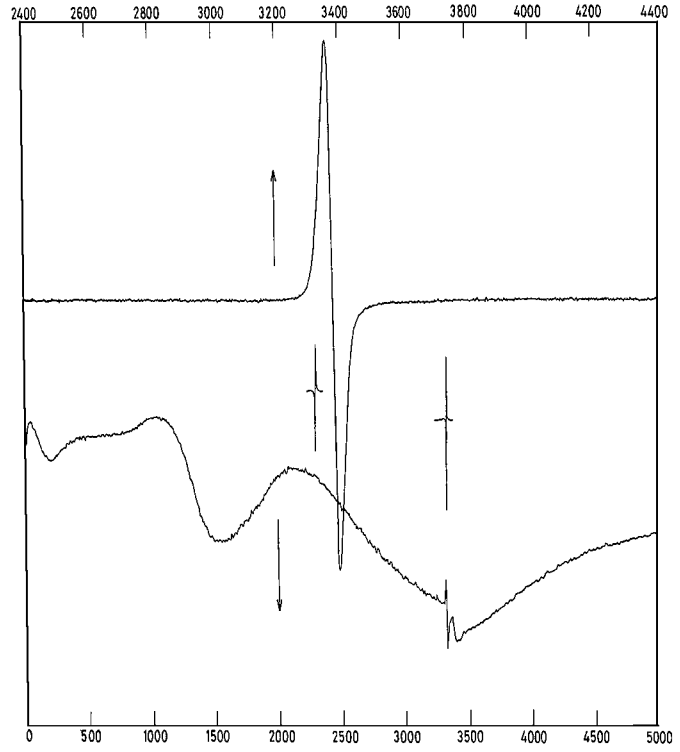

FIG. 5. EPR spectra of CrSiAl sample before (top) and after (bottom) ODH of propane.

same for all the catalysts, but the ΔH value varies slightly for the different supports. The presence of crystal β-Cr^{3+} ($g = 1.95$, $\Delta H = 700$–800 G) due to Cr_2O_3 microcrystals was observed for 10% CrAl and 4% CrTi, and for higher loadings on Al_2O_3 and TiO_2 supports. However, for the CrSi and CrSiAl catalysts the crystal β-Cr^{3+} EPR peak was not detected even up to 5% Cr_2O_3 loading.

The EPR spectra for the 1% CrSiAl catalyst before and after ODH of propane are shown in Fig. 5. In the EPR spectrum of the sample after reaction (bottom spectrum) a broad peak corresponding to β-Cr^{3+} ($g = 2.41$, $\Delta H = 1200$ G) along with a weak signal corresponding to γ-Cr^{5+} was observed. Furthermore, the δ-Cr^{3+} ($g \sim 4.43$) centered around 1500 G was also present in the EPR spectra after reaction.

UV–Vis DRS Studies

The UV–vis DRS spectra of the CrAl samples were obtained under ambient and dehydrated conditions. The spectra in terms of the Kubelka–Munk function versus wavelength for the samples under different conditions are shown in Fig. 6A for 1% CrAl and in Fig. 6B for 10% CrAl. From Fig. 6A it is observed that the ambient DRS spectra have two transitions, at 287 and 370 nm. These peaks correspond to Cr^{6+}–O^{2-} charge transfer transitions for the chromate species (34). The dehydrated DRS spectra exhibit a slight shift for the above peaks at 500°C in pure oxygen, to 295 and

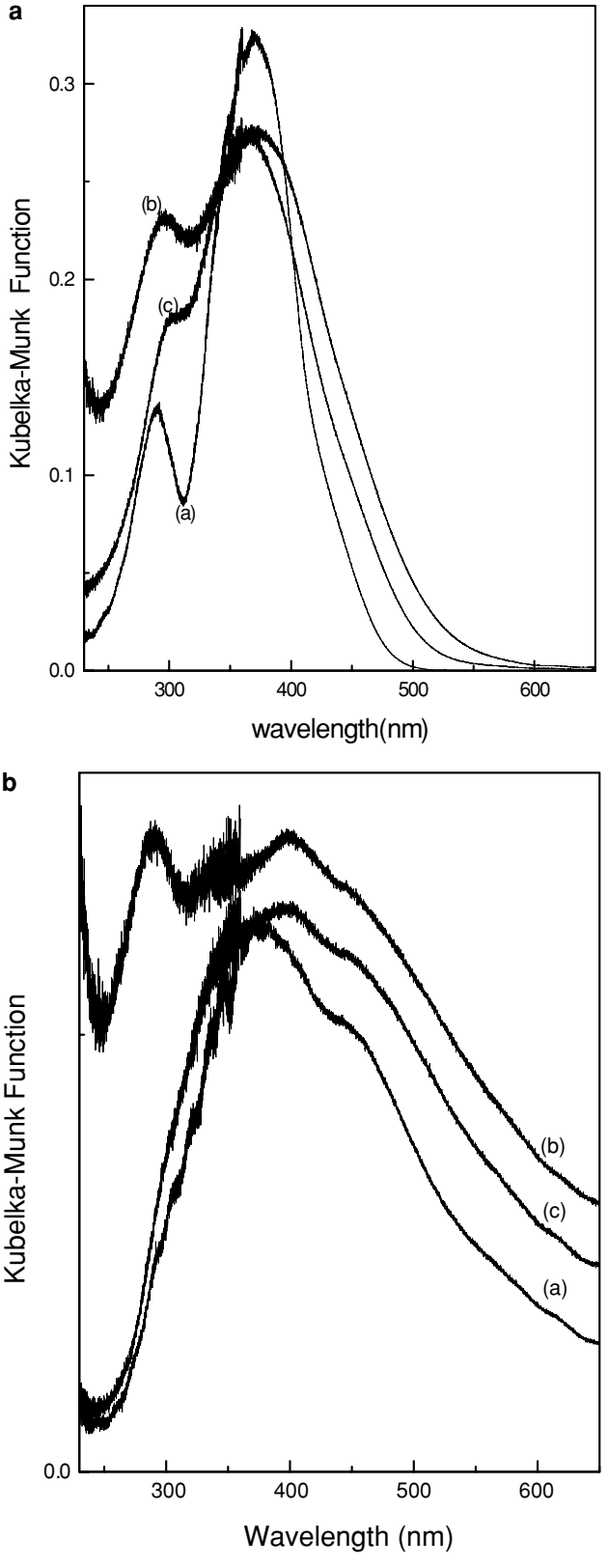

FIG. 6. (A) UV–vis DRS of 1% CrAl under different conditions. (a) Ambient; (b) 500°C in oxygen; (c) room temperature in oxygen. (B) UV–vis DRS of 10% CrAl under different conditions. (a) Ambient; (b) 500°C in oxygen; (c) room temperature in oxygen.

TABLE 4

Peak Positions in the DRS Spectra of *x*% CrAl Samples Under Different Conditions

Wt% CrAl	Peak positions (nm)		
	Ambient	500°C (in oxygen)	RT (in oxygen)
0.5	284, 370	292, 363	300, 358
1	287, 370	295, 370	304, 372
5	380	282, 399	390
10	373, 456	290, 401	385, 454
15	373, 456, 586	280, 396, 588	370, 580
20	370, 452, 578	280, 396, 460, 580	374, 470, 583

372 nm, respectively. After cooling to room temperature in pure oxygen the peaks shift to 304 and 368 nm. The DRS spectra of 10% CrAl under the same conditions are shown in Fig. 6b. Under ambient conditions a peak at ~370 nm was observed along with a shoulder at ~450 nm. At 500°C in pure oxygen, a peak is also observed at 290 nm, similarly to the 1% CrAl spectrum. After cooling to room temperature in pure oxygen the low wave number band shifts to ~401 nm but the shoulder is still present at ~450 nm. The peak positions in the DRS spectra of the other *x*% CrAl samples for different conditions are tabulated in Table 4. From Table 4 it is observed that for the dehydrated UV–vis DRS spectra at 500°C, in addition to the Cr^{6+}–O^{2-} charge transfer transition peaks, an intense peak between 280 and 292 nm was detected that was independent of chromia loading. It is difficult to assign this 280- to 292-nm peak to a particular oxidation state since the octahedral *d-d* transitions for Cr^{4+} and Cr^{5+} are identical to other existing chromium oxide species, such as Cr^{3+} and Cr^{6+} (21).

The UV–vis DRS spectrum for the 5% CrAl sample at 500°C in a 30% C_3H_8 + He flow is shown in Fig. 7, along with the spectrum obtained in pure oxygen at 500°C for the same sample. The 370-nm peak is totally absent after reduction; however, the peak at about 280 nm remains unaffected. Similar spectra were observed with other CrAl samples. The intensity of the 280-nm peak after the reduction experiments is plotted against the mole fraction of Cr in Fig. 8. The intensity of the 280-nm peak after propane reduction increases linearly with the mole fraction of Cr. Thus, it appears that the surface Cr oxide species corresponding to the 280-nm UV–vis DRS peak does not participate in the reaction and its concentration increases with loading at least up to 0.003 mol fraction of Cr.

TPR Studies

TPR studies were performed on the different supported chromia catalysts. The pure oxide supports (Al_2O_3, TiO_2, SiO_2, and SiO_2–Al_2O_3) did not reveal any reduction under the experimental conditions considered in the present

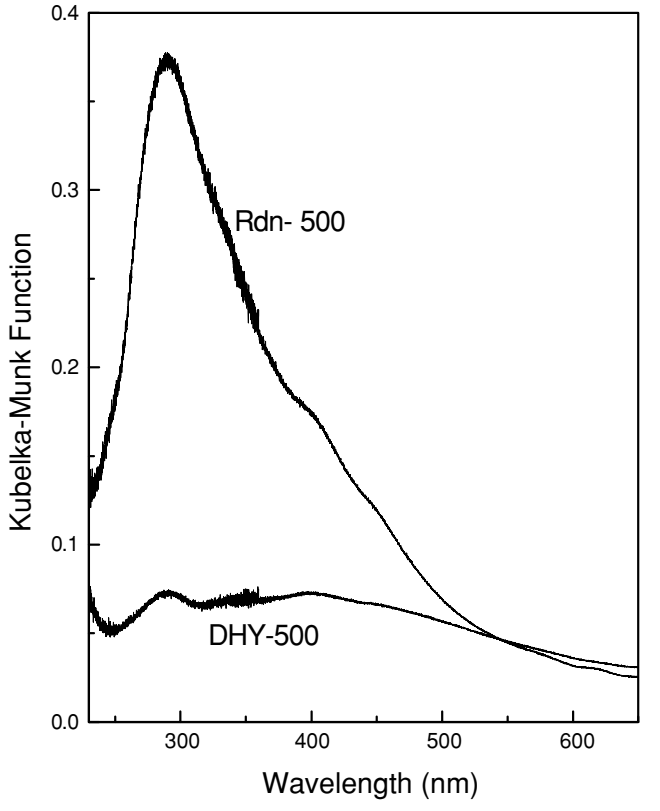

FIG. 7. UV–vis DRS of 5% CrAl under fully oxidized (DHY-500) and reduced conditions (Rdn 500). Reduction achieved in 30% C_3H_8 + helium.

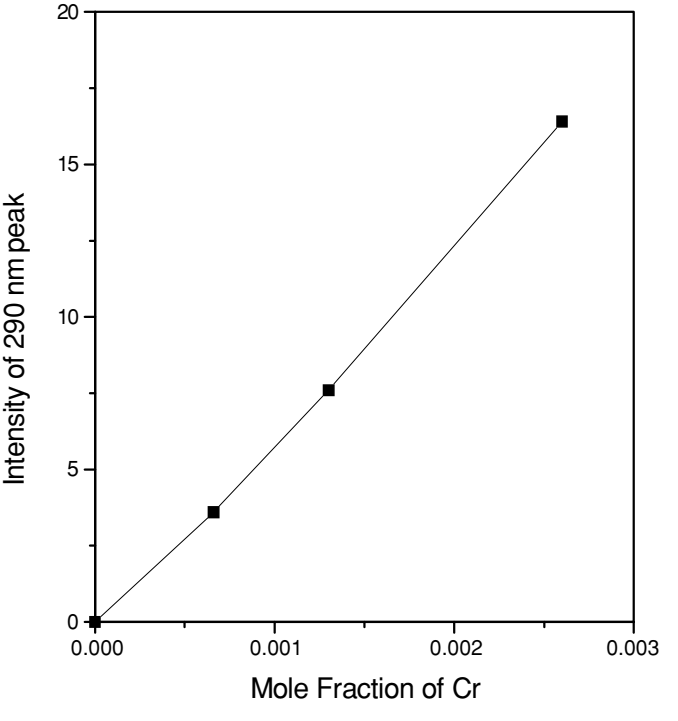

FIG. 8. Intensity of 290-nm peak from DRS versus mole fraction of Cr for the CrAl catalysts.

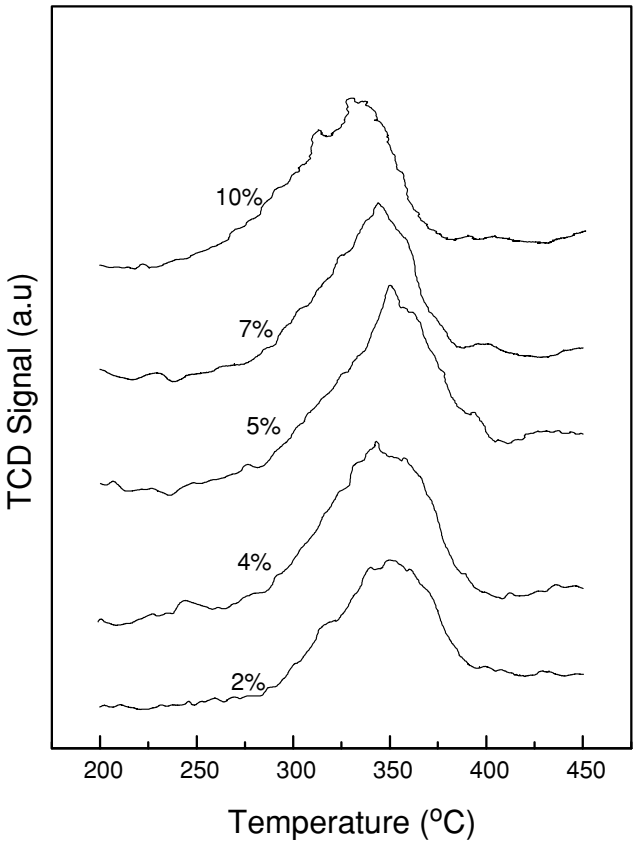

FIG. 9. TPR profiles of x% CrTi catalysts.

study. For illustration purposes, the TPR profiles for x% CrTi samples are plotted versus the temperature in Fig. 9. A single peak, or T_{max} temperature, is present and suggests a single reduction step. Furthermore, from the peak area and calibration amounts of hydrogen, the hydrogen consumption can be calculated, which is then used to calculate the H/Cr ratio. Consequently, from TPR experiments the T_{max} temperature and H/Cr ratios can be determined. These values are tabulated in Table 5 for the CrAl, CrTi, CrSi, and CrSiAl catalysts. From the data presented in Table 5 it is observed that the T_{max} temperature of the supported chromium oxide species appears to be relatively independent of chromia loading but strongly dependent on the specific support used. The T_{max} temperatures for the CrTi samples varied from 342 to 351°C and for the CrSi samples from 433 to 445°C. The T_{max} temperature for CrAl and CrSiAl catalysts was similar, between 388 and 365°C. Furthermore, the H/Cr ratio appears to be relatively constant, ~2, for low loading of chromium oxide but decreases for high loadings, with the exception of the CrSi catalysts, for which there was a significantly smaller value.

ODH of Propane

The propane ODH studies for the pure oxide supports and the different supported chromium oxide catalysts were performed at temperatures ranging from 380 to 500°C. Under the operating conditions employed in the present study the pure supports were inactive for the ODH of propane. For comparative purposes the activity, selectivity, and TOF data for all the supported chromia samples are tabulated at 400°C in Table 6. For all the supported chromia catalysts, the catalytic activity initially increases with an increase in chromia loading, and after reaching a maximum the catalytic activity decreases for higher chromia loadings. However, there is no general trend in selectivity for all the supported chromia catalysts. For the CrAl catalysts, the catalytic activity also increases up to 15% Cr_2O_3 loading and decreases for higher chromia loadings. The selectivity to propene is observed to follow the same trend as that of the conversion-versus-chromia loading for the CrAl samples. The selectivity increases with loading up to 15% Cr_2O_3 and decreases for higher chromia loading. For the CrTi catalysts, the activity also increases with chromia loading up to 5% Cr_2O_3 loading and decreases upon further increase in chromia loading. However, unlike the CrAl samples the selectivity to propene continuously increases with loading, from 59 to 73%, and then remains constant at ~70%. For the CrSi catalysts, catalytic activity increases as the loading is increased from 0.5 to 1% Cr_2O_3 loading and decreases for 2% and higher Cr_2O_3 loadings. The selectivity to propene for the CrSi samples remains relatively constant, at 50 to 58%, for the different chromium oxide loading. For the CrSiAl catalysts the maximum activity was obtained for the 2% CrSiAl catalyst. With an increase in chromia

TABLE 5

T_{max} and H/Cr Values from TPR Studies of the Supported Chromium Oxide Catalysts

CrAl			CrTi			CrSi			CrSiAl		
Wt%	T_{max} (°C)	H/Cr	Wt%	T_{max} (°C)	H/Cr	Wt%	T_{max} (°C)	H/Cr	Wt%	T_{max} (°C)	H/Cr
5	388	1.9	2	350	2.1	0.5	445	1.1	1	380	ND[a]
7.5	374	1.6	3	351	2.0	1	440	n.d	2	375	2.02
10	373	1.5	4	347	1.3	2	435	0.84	5	365	1.22
15	377	1.3	5	342	1.1	5	443	0.22			

[a] ND, Not determined.

TABLE 6

Activity, Selectivity, and TOF for Supported Chromium Oxide Catalysts at 400°C[a]

CrAl				CrTi				CrSi				CrSiAl			
Wt%	Activity, $\times 10^6$ (mol/g·s)	Selectivity (%)	TOF (s^{-1}), $\times 10^3$	Wt%	Activity, $\times 10^6$ (mol/g·s)	Selectivity (%)	TOF (s^{-1}), $\times 10^3$	Wt%	Activity, $\times 10^6$ (mol/g·s)	Selectivity (%)	TOF (s^{-1}), $\times 10^3$	Wt%	Activity, $\times 10^6$ (mol/g·s)	Selectivity (%)	TOF (s^{-1}), $\times 10^3$
5	1.2	63	1.9	2	1.1	59	4.4	0.5	0.62	50	9.5	0.5	0.3	30	1.6
7.5	1.7	73	1.8	3	1.7	68	4.3	1	1.1	58	8.3	1	0.6	36	2.0
10	2.3	72	1.7	4	2.3	73	4.3	2	0.63	50	2.4	2	0.8	50	2.4
15	3.2	78	1.6	5	2.5	70	3.8	5	0.73	55	1.04	5	0.7	55	0.6
20	1.7	72	0.7	7	1.3	71	1.3								

[a] Conditions: $C_3H_8 : O_2 = 3 : 1$.

loading in the CrSiAl samples, the selectivity increases from 30 to 50% and then remains relatively constant. The TOF values of the supported chromium oxide samples are relatively constant with chromia loading, except for 20% CrAl, 7% CrTi, 2 and 5% CrSi, and 5% CrSiAl samples. TOF values significantly decrease for these high-loading samples.

The TOF values of the 1 wt% Cr_2O_3 on Al_2O_3, TiO_2, SiO_2, and SiO_2–Al_2O_3 catalysts are plotted against temperature in Fig. 10 and, as expected, increase with temperature. Similar variations in TOF with temperature for other supported chromia catalysts possessing dispersed chromia species were observed. Furthermore, it is observed from Fig. 10 that the TOF values for CrSi and CrTi catalysts are similar while the TOF values for CrSiAl and CrAl catalysts are also similar. It is interesting that the selectivity for the chromia supported on alumina, titania, and silica–alumina catalysts increased with temperature up to 500°C. The selectivity slightly decreased at tempertures higher than 400°C for chromia supported on silica catalysts. The increase in selectivity to propene was observed due to the increased amount of propene compared to the amount of carbon oxide formed at higher temperatures. Based on the temperature effects and differential conditions the activation energies were calculated for total conversion of propane. For the CrAl and CrSiAl samples, E_a varied between 90 and 100 kJ/mol and that for the CrTi and CrSi catalysts varied between 110 and 120 kJ/mol.

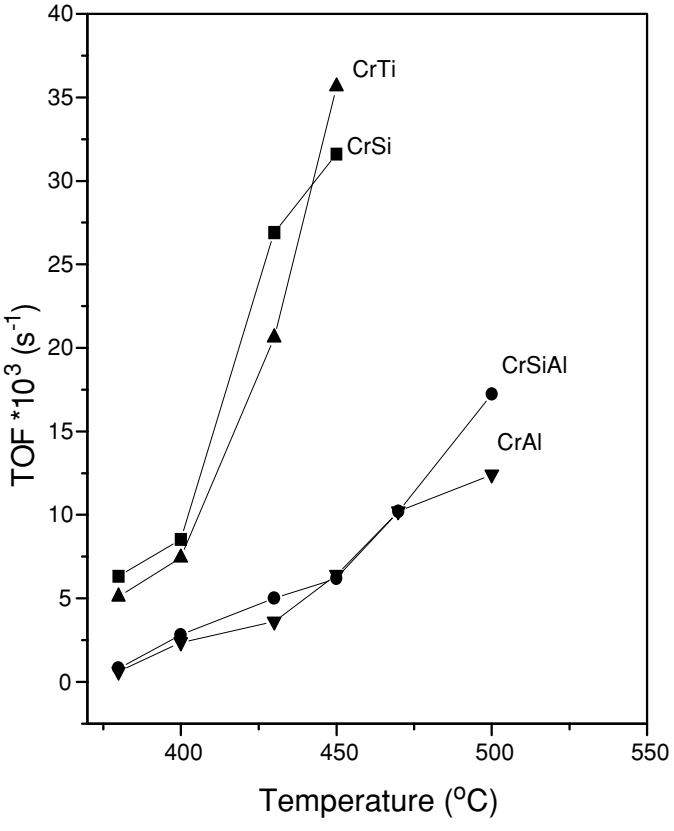

FIG. 10. TOF versus temperature for 1% Cr_2O_3 loading on SiO_2, TiO_2, Al_2O_3, and SiO_2–Al_2O_3 supports.

DISCUSSION

Surface chromium oxides sites are formed on the Al_2O_3, TiO_2, SiO_2, and SiO_2–Al_2O_3 supports up to monolayer surface coverages. The monolayer coverages were defined as the loading at which Cr_2O_3 microcrystals were first detected. The presence of Cr_2O_3 crystals is ideally detected by Raman spectroscopy under ambient and dehydrated conditions, since its Raman band at ~557 cm^{-1} is sharp and distinct. From the Raman spectra, monolayer surface chromium oxide coverages on the Al_2O_3, SiO_2, and SiO_2–Al_2O_3 supports used in the present study were determined to be less than 15, 2, and 3% Cr_2O_3 loading, respectively. Monolayer loadings could not be determined by Raman spectroscopy for the CrTi samples due to the strong Raman vibrations of the TiO_2 support below 800 cm^{-1}. XPS studies can also be used for determining the monolayer coverage. The plateauing of plots of $Cr/(Cr + S)_{surface}$ versus $Cr/(Cr + S)_{bulk}$ from XPS analysis have been attributed to crystalline formation (35) and the point of transition where the plateau occurs is approximated as the

monolayer coverage. From such XPS analysis, monolayer coverages for the supported chromia catalysts were obtained and the corresponding values for the CrAl, CrTi, and CrSiAl samples were determined to be ~12, ~4, and ~3% Cr_2O_3 respectively. For the CrSi samples the monolayer limit was difficult to determine since the $Cr/(Cr + S)_{surface}$ versus $Cr/(Cr + S)_{bulk}$ does not reveal a clear transition. The UV–vis DRS spectra for 15 and 20% Cr_2O_3 loadings also reveal Cr^{3+} *d-d* transitions at 570 nm due to Cr_2O_3 crystallites. Consequently, from a combination of Raman, XPS and UV–vis DRS studies the monolayer coverages on these supports was determined to be ~12, ~4, ~1, and ~3% Cr_2O_3 on Al_2O_3, TiO_2, SiO_2, and SiO_2–Al_2O_3 supports, respectively. Based on the surface area of the oxide support these surface chromia loadings correspond to surface densities of ~8, ~9, ~2.5, and ~1.1 μmol Cr/m^2 (~5, ~5.6, ~1.6, and ~0.7 Cr atoms/nm^2), respectively. Thus, the monolayer surface coverages on Al_2O_3 and TiO_2 are similar and much greater than the monolayer coverages on SiO_2 and SiO_2–Al_2O_3 due to weak interaction between silica and chromia. The surface density values correspond to what was found for other supported metal oxides on these supports.

Below monolayer chromia loadings, the chromium oxide is present as two-dimensional dispersed surface species. The presence of the dispersed species is directly monitored in the Raman and diffusive reflectance spectra. In the hydrated Raman spectra, the bands at 840–850 cm^{-1} correspond to chromium–oxygen vibrations that are present irrespetive of specific oxide support and chromia loading. This Raman band is assigned to hydrated surface Cr^{6+} species present in the form of chromates with different degrees of oligomerization (32). Dehydrated Raman spectra also reveal bands at ~1030 and ~1010 cm^{-1} for supported chromia catalysts, with the exception of the CrSi samples. The Raman bands at ~1030 and ~1010 cm^{-1} are due to the terminal mono–oxo Cr=O bond (30) of dehydrated CrO_4 monochromates and polychromates, respectively. The intense Raman band at 980 cm^{-1} obtained under dehydrated conditions for the CrSi catalyst is assigned to the isolated symmetric CrO_2 functionality present on the SiO_2 support (30). Furthermore, the hydrated and dehydrated UV–vis DRS spectra for the CrAl catalysts suggest the presence of surface Cr^{6+} species due to the electronic transition observed at 370 nm.

In addition to the Cr^{6+} oxide species detected, EPR analysis reveals the presence of some Cr^{5+} species in all the prepared samples before reaction. The concentration of the Cr^{5+} was observed to decrease with an increase in chromia. For chromia loadings higher than monolayer coverage, quantification of the surface Cr^{5+} species was difficult since strong β-Cr^{3+} species dominate the EPR spectra. In addition to the Cr^{5+} and Cr^{6+} species, it appears that some dispersed δ-Cr^{3+} is also present on the TiO_2, SiO_2, and SiO_2–Al_2O_3 supports. Thus, it appears that in addition to the surface Cr^{6+} oxide species detected from Raman and UV–vis DRS studies, some Cr^{5+} and δ-Cr^{3+} species are also present in these oxide supports under ambient conditions after calcinations.

The TPR analysis reveals that chromium oxide supported on alumina, titania, silica, and silica–alumina catalysts are reducible and different fom bulk. The T_{max} temperature and H/Cr value for bulk Cr_2O_3 are 292°C and 0.7, respectively (36). The reducibility of the surface chromium oxide species, which is represented by the T_{max} temperature, is strongly dependent on the specific oxide support and increases in the following order: $TiO_2 < [SiO_2$–$Al_2O_3] \sim Al_2O_3 < SiO_2$. Thus, the oxygen is more strongly bound in the chromium oxide supported on SiO_2 and Al_2O_3 compared to TiO_2 with respect to H_2 reduction. The H/Cr ratio was relatively independent of chromia loading and support up to monolayer suface coverage but is different from the value of 3 required for the reduction of chromium oxide from a +6 oxidation state to +3. Therefore, the TPR data suggests that a constant fraction of total Cr species below monolayer loadings is undergoing reduction independently of the loading and support; however, the ease of reduction by H_2 is strongly dependent on the support.

The ambient EPR spectra before and after ODH of propane revealed that Cr^{5+} species are present both before and after reaction. Since EPR spectroscopy is extremely sensitive, the detection of paramagnetic species are most likely due to their presence in trace amounts. Furthermore, δ-Cr^{3+} species was observed on some of the samples, which is also not affected by reduction–oxidation. Consequently, it appears that Cr^{5+} and δ-Cr^{3+} form part of the irreducible chromium oxide species present, which may be the reason that the H/Cr ratio is less than 3. Additionally, as observed from *in situ* UV–vis DRS spectra, the peak at 280 nm remains unaffected during propane reduction; however, the peak corresponding to 370 nm disappears completely during propane reduction at 500°C. Correlating the EPR and *in situ* UV–vis DRS data suggests that the Cr^{5+} signal, which remains unchanged before and after reaction, is related to the 280-nm peak, which is also unaffected by reduction.

The propane ODH reacitivity studies reveal that the activity and selectivity of the supported chromium oxide catalysts depends on the chromia loading and the oxide support used. As the chromia loading is increased, the ODH activity initially increases and then decreases. The catalytic activity exhibited maxima with 15% CrAl, 5% CrTi, 1% CrSi, and 2% CrSiAl catalysts, which correspond to monolayer surface coverages. As the chromia loading increases above monolayer surface coverage, the presence of bulk Cr_2O_3 crystals increases and the activity decreases. Previous studies reveal that the chromia species in crystalline Cr_2O_3

is less active than the two-dimensional surface chromia phase that is present below monolayer surface coverages (36). Additionally, the number of surface chromia species is decreased when crystalline Cr_2O_3 is formed. Hence, above monolayer coverages the activity decreases. Analysis of the activity data given in Table 6 reveals that the activity of the surface chromium oxide phase is strongly dependent on the support. Much higher activity values were achieved on CrAl and CrTi catalysts compared to that on CrSi and CrSiAl catalysts. Also, for the same surface coverages the CrAl catalysts show higher conversion followed by CrTi catalysts. This difference is activity values is directly related to the larger concentration of surface chromium oxide species that can be supported on the Al_2O_3 and TiO_2 supports compared to that on the SiO_2 and SiO_2–Al_2O_3 supports.

The propane ODH selectivity to propene for the different supported chromium oxide catalysts increases with loading and appears to reach a constant value at monolayer surface coverages. This trend suggests that the exposed oxide support surface sites degrade propene to carbon oxides since they are not active for propane activation. Furthermore, the maximum selectivity is achieved for the CrAl and CrTi catalysts since at monolayer chromia loadings an insignificant amount of the support surface is exposed. For the CrSi and CrSiAl catalysts the maxium selectivity pattern is similar, but it is lower than the CrAl and CrTi catalysts because exposed support sites present for CrSi and CrSiAl degrade propene to carbon oxides.

The TOF of the surface chromia site present in the supported chromium oxide catalysts follows the order CrTi $\cong$ CrSi > CrSiAl $\geq$ CrAl. The TOF represents the intrinsic activity of each surface chromia site. This trend in TOF values is applicable for all submonolayer coverages of the supported chromium oxide catalysts. The TOF values do not change with respect to Cr_2O_3 loading below monolayer coverages. These constant TOF values for the supported chromia catalysts with surface chromia coverage demonstrate that only one surface chromia site is required for propane ODH to propylene. Similar conclusions were reached for propane ODH over supported vanadia catalysts (37). The trend in TOF values as the support is changed, however, does not follow the reducibility of the surface chromium oxide species, as observed from H_2 TPR studies, since the T_{max} temperature follows the order CrSi > CrAl ~ CrSiAl > CrTi. Thus, it appears that the oxygen bonding to the support is not the only parameter that is important for the ODH of propane. The reason for this apparent discrepancy is that on SiO_2 different chromium oxide species are present, as is observed by Raman spectroscopy (30). The dehydrated surface chromium oxide species on silica exhibits Raman bands at 986 cm^{-1}, whereas on titania and alumina supports the Raman bands are present at 1000–1005 cm^{-1}. It appears that this difference in the nature of the dehydrated surface chromium oxide species plays a significant role in the TOF of the CrSi catalysts.

The redox properties of chromium oxide on SiO_2 under various conditions for different reactions have been reported (13, 38–41). Furthermore, various studies on ODH of propane over silica-supported vanadia catalysts suggested that V_2O_5/SiO_2 is a promising catalyst for ODH (42, 43). Bellusi *et al.* (44) proposed the involvement of surface silanol groups with weak basic character in the reaction mechanism. Based on these observations it appears that the mechanism of propane ODH over CrSi catalysts may also be different from that on CrTi, CrAl, and CrSiAl catalysts, which gives rise to a higher TOF value for the CrSi catalysts.

Comparison of the TOF and selectivity of propane ODH and TPR results suggests that the surface chromium oxide species on the SiO_2–Al_2O_3 support behaves similar to the Al_2O_3 support. This is not surprising since it is known that surface chromium oxide species migrate away from the SiO_2 surface to the Al_2O_3 surface (45). Furthermore, since only 3% CrSiAl corresponds to a monolayer (surface area = 360 m^2/g), only small domains of Al_2O_3 separated by larger SiO_2 domains appear to be present on the surface of the SiO_2–Al_2O_3 support.

The characterization studies on supported chromium oxide catalysts revealed that Cr^{6+}, Cr^{5+}, and dispersed Cr^{3+} are present. Hakuli *et al.* (46) proposed that the active species for the dehydrogenation reaction are redox Cr^{3+} sites and exposed nonredox Cr^{3+}. De Rossi *et al.* have also suggested that Cr^{3+} is the active site (12). Pradier *et al.* (4) proposed that the nanocrystals of Cr_2O_3 present on supported chromia catalysts are active for complete oxidation reaction. Studies by Cavani *et al.* (14) reveal that the activity of reduced Cr^{3+} was less than dispresed Cr^{3+} species for the dehydrogenation of isobutane. Recent studies involving modified chromium oxide sites reveal that the Cr^{5+} species are inactive for the ODH of propane reaction (47). On the assumption a redox mechanism occurs, the reduction–oxidation cycle between the Cr^{6+}, which corresponds to the 370-nm peak in the UV–vis DRS, and the Cr^{3+} species, which corresponds to $g = 2.4$ and is centered at ~1200 G in the EPR, is the active site for the ODH of propane.

In summary, the structure–reactivity/selectivity relationships reveal that the surface chromium oxide species are similar on the TiO_2, Al_2O_3, and SiO_2–Al_2O_3 supports. However, as observed from the Raman spectra obtained under dehydrated conditions, the surface chromium oxide species on SiO_2 is different. It appears that this difference in surface chromium oxide species on SiO_2 gives rise to a different mechanism for the propane ODH reaction and a high TOF value. Limitations using SiO_2 as a support exist since the maximum surface chromia density is significantly

lower than those achieved on TiO_2 and Al_2O_3 supports. Consequently, a much higher yield of propene is achieved on the chromium oxide supported on Al_2O_3 or TiO_2 catalysts. Comparison of the catalytic data of the CrAl and CrTi catalysts suggests that a higher propene yield is achieved for the CrAl catalysts. This is due to the larger surface area of the Al_2O_3 support, which accommodates a large amount of dispersed chromium oxide species. A comparable surface area of TiO_2 support would be able to accommodate larger Cr_2O_3 loadings at monolayer coverages and give rise to a higher activity and yield. Consequently, the chromium oxide species on the TiO_2 support is the most suitable for the ODH of propene.

CONCLUSIONS

Supported chromia catalysts are prepared by the incipient wetness impregnation method on Al_2O_3, TiO_2, SiO_2, and SiO_2–Al_2O_3 supports. The calcined samples were characterized for their BET surface areas and by ambient and dehydrated Raman, XPS, EPR, TPR, and UV–vis DRS spectroscopic techniques. The presence of surface Cr (+6) chromates was confirmed by Raman, XPS, and UV–vis DRS studies. Microcrystals of Cr_2O_3 were detected above monolayer surface coverage. Monolayer surface coverages are 8–9 μmol of Cr/m^2 for Al_2O_3 and TiO_2, but 1–3 μmol of Cr/m^2 for the SiO_2 and SiO_2–Al_2O_3 supports. In addition to the surface Cr^{+6} species, small amounts of Cr^{5+} and δ-Cr^{3+} species, which are unaffected during the reaction, are also present. The dehydrated Raman spectra revealed the presence of isolated surface monochromate species in the CrSi samples and both surface monochromate and polychromate species in the CrAl and CrTi samples.

The reactivity studies during propane ODH for the supported chromia catalysts suggested that activity and selectivity strongly depend on the chromia loading and the specific oxide support. The propane conversion and propene selectivity increase with chromia loading up to monolayer surface coverages. The intrinsic activities of the surface chromium oxide species, the TOF values, for the different support chromia catalysts varied by an order of magnitude and increased in the order $CrAl \cong CrSiAl < CrSi \cong CrTi$. The TOF of the supported chromium oxide catalysts, however, was independent of coverage for a specific oxide support. The constant TOF values with surface chromia coverages up to a monolayer demonstrate that only one surface Cr site is required for the propane ODH reaction to propylene.

ACKNOWLEDGMENTS

Prof. Jih-Mirn Jehng, Department of Chemical Engineering National Chung Hsing University, Taiwan, and Dr. Prem Chand, Department of Physics, Indian Institute of Technology, Kanpur, India, are gratefully acknowledged for assisting in the Raman and EPR studies. This work at IIT Kanpur has been partially supported by financial assistance from the Department of Science and Technology, India. Financial support by the United States Department of Energy–Basic Energy Sciences for the studies performed at Lehigh University is gratefully acknowledged.

REFERENCES

1. Kung, H. H., *Adv. Catal.* **40**, 1 (1995).
2. Haber, J., *in* "Handbook of Heterogeneous Catalysis," Vol. 2, p. 2258, 1997.
3. Delmon, B., Ruiz, P., Carrazan, S. R. G., Korili, S., Vicente Rodriguez, M. A., and Sobalik, Z., "Catalysis in Petroleun Refining and Petrochemical Industries." Elsevier Science, B.V. NY. 1995.
4. Pradier, C. M., Rodrigues, F., Marcus, P., Landau, M. V., Kaliya, M. L., Gutman, A., and Herskowitz, M., *Appl. Catal. B* **27**, 73 (2000).
5. Wachs, I. E., *Catal. Today* **27**, 437 (1996).
6. Blasco, T., and Lopez Nieto, J. M., *Appl. Catal. A* **157**, 117 (1997).
7. Mamedov, E. A., and Corberan, V. C., *Appl. Catal. A* **127**, 1 (1995).
8. Khodakov, A., Yang, J., Su, S., Iglesia, E., and Bell, A. T., *J. Catal.* **177**, 343 (1998).
9. Chen, K., Xie, S., Iglesia, E., and Bell, A. T., *J. Catal.* **189**, 421 (2000).
10. Chen, K., Xie, S., Bell, A. T., and Iglesia, E., *J. Catal.* **198**, 232 (2001).
11. Lugo, H. J., and Lunsford, J. H., *J. Catal.* **91**, 155 (1985).
12. De Rossi, S., Ferraris, G., Fremiotti, S., Garrone, E., Ghiotti, G., Campa, M. C., and Indovina, V., *J. Catal.* **148**, 36 (1994).
13. Udomsak, S., and Anthony, R. G., *Ind. Eng. Chem. Res*. **35**, 47 (1996).
14. Cavani, F., Koutyrev, M., Trifiro, F., Bartolini, A., Ghisletti, D., Iessi, R., Santucci, A., and Delpiero, G., *J. Catal.* **158**, 236 (1996).
15. Gorriz, O. F., and Cadus, L. E., *Appl. Catal. A* **180**, 247 (1999).
16. Grzybowska, B., Sloczynki, J., Grabowski, R., Wcislo, K., Kozlowska, A., Stoch, J., and Zielinski, J., *J. Catal.* **178**, 687 (1998).
17. Al-Zahrani, S. M., Elbashir, N. O., Abasaeed, A. E., and Abdulwahed, M., *Ind. Eng. Chem. Res.* **40**, 781 (2001).
18. Hoang, M., Mathews, J. E., and Pratt, K. C., *React. Kinet. Catal. Lett.* **61**(1), 21 (1997).
19. Grabowski, R., Grzybowska, B., Stoczynski, J., and Wcislo, K., *Appl. Catal. A* **144**, 335 (1996).
20. Stoczynski, J., Grzybowska, B., Grabowski, R., Koztowska, A., and Wcislo, K., *Phys. Chem. Chem. Phys.* **1**, 333 (1999).
21. Khadder-Zine, S., Ghorbel, A., and Naccache, C., *J. Mol. Catal.* **150**, 223 (1999).
22. Rahman, A., Mohamed, M. H., Ahmmed, M., and Aitani, A. M., *Appl. Catal. A* **121**, 203 (1995).
23. Scierka, S. J., Houlla, M., Proctor, A., and Hercules, D. M., *J. Phys. Chem.* **99**, 1537 (1995).
24. Vuurman, M. A., Stufkens, D. J., Oskam, A., Moulijn, J. A., and Kapteijn, F., *J. Mol. Catal.* **60**, 83 (1990).
25. Weckhuysen, B. M., Wachs, I. E., and Schoonheydt, R. A., *Chem. Rev.* **96**, 3327 (1996).
26. Weckhuysen, B. M., and Wachs, I. E., *J. Phys. Chem.* **100**, 14437 (1996).
27. Weckhuysen, B. M., Jehng, J-.M., and Wachs, I. E., *J. Phys. Chem. B* **104**, 7382 (2000).
28. Bond, G. C., "Handbook of Heterogeneous Catalysis," Wiley-VCII, Weinheim, Vol. 1, p. 792, 1997.
29. Zaki, M. I., Fouad, N. E., Bond, G. C., and Tahir, S. F., *Thermochim. Acta* **285**, 167 (1996).
30. Vuurman, M. A., Wachs, I. E., Stufkens, D. J., and Oskam, A., *J. Mol. Catal.* **80**, 209 (1993).
31. Froment, G. F., and Bischoff, K. B., "Chemical Reactor Analysis and Design," 2nd ed., John Wiley & Sons, New York, 1990.
32. Vuurman, M. A., Stufkens, D. J., Oskam, A., Moulijn, J. A., and Kapteijn, F., *J. Mol. Catal.* **60**, 83 (1990).

33. El-Edrissi, J., Kacimi, M., Venduraz, F. B., and Ziyad, M., *Catal. Lett.* **56**, 221 (1998).
34. Weckhuysen, B. M., De Ridder, L. M., and Schoonheydt, R. A., *J. Phys. Chem.* **97**, 4756 (1993).
35. Kerkhof, F. P. J. M., Moulijn, J. A., and Thomas, R., *J. Catal.* **56**, 279 (1979).
36. Cherian, M., Rao, M. S., Yang, W. T., Jehng, J.-M., Hirt, A. M., and Deo, G., *Appl. Catal. A* **233**, 21 (2002).
37. Gao, X., and Wachs, I. E., *Appl. Catal.* **209**, 43 (2002).
38. Kim, D. S., Tatibouet, J. M., and Wachs, I. E., *J. Catal.* **136**, 209 (1992).
39. Hakuli, A., Harlin, M. E., Backman, L. B., and Krause, A. O. I., *J. Catal.* **184**, 349 (1999).
40. Bensalem, A., Weckhuysen, B. M., and Schoonheydt, R. A., *J. Phys. Chem. B* **101**, 2824 (1997).
41. Wang, S., Murata, K., Hayakawa, T., Hamakawa, S., and Suzuki, K., *Appl. Catal.* **196**, 1 (2000).
42. Parmaliana, A., Sokolovski, V., Miceli, D., and Giordane, N., *Appl. Catal.* **135**, L1 (1996).
43. Le Bars, J., Vedrine, J. C., and Auroux, A., *Appl. Catal. A* **88**, 179 (1992).
44. Bellusi, G., Centi, G., Perathoner, S., and Trifiro, F., *in* "Catalytic Selective Oxidation," p. 281. Am. Chem. Soc. Washington, DC, 1993.
45. Weckhuysen, B. M., Schoofs, B., and Schoonheydt, R. A., *J. Chem. Soc. Faraday Trans.* **93**, 2117 (1997).
46. Hakuli, A., Kytokivi, A., and Krause, A. O. I., *Appl. Catal. A* **190**, 219 (2000).
47. Cherian, M., Gupta, R., Rao, M. S., and Deo, G., submitted for publication.